Investigation of BARC-Resist Interfacial Interactions

Chelladurai Devadoss[a], Yubao Wang[a], Rama Puligadda[a], Joseph L. Lenhart[b], Erin L. Jablonski[c], Daniel A. Fischer[d], Sharadha Sambasivan[c], Eric K. Lin[c], Wen-Li Wu[c]
[a]Brewer Science, Inc., Rolla, MO 65401
[b]Sandia National Laboratory, Albuquerque, NM 87185
[c]Polymers and [d]Ceramics Divisions, National Institute of Standards and Technology, Gaithersburg, MD 20899

ABSTRACT

With the increasing drive towards smaller feature sizes in integrated circuits and the consequent use of shorter exposure wavelengths, the imaging resist layer and underlying bottom anti-reflective coating (BARC) layer are becoming thinner. At this scale, the performance of chemically amplified resists can be adversely affected by the BARC-resist interfacial interactions. These interactions can cause distortion of resist profiles and lead to footing, undercut, or pattern collapse. BARC components can immensely influence the deprotection and dissolution properties of the resist. A thorough understanding of the physico-chemical interactions at these interfaces is essential to design and develop new material platforms with minimal adverse interactions and maximum compatibility between BARC and resist. Results are reported from studies of (A) surface versus bulk chemistry of BARC materials as a function of cure temperature, (B) the dependence of the thickness and composition of the residual layer (resist material remaining on the surface of the BARC after development) on BARC components, as determined by formulating the BARC or resist with an excess of various BARC components, and (C) the dependence of the residual layer thickness on crosslink density, exposure dose, and resist bake temperature. The BARC thin films and the interphase between BARC and resist were characterized with near edge x-ray absorption fine structure (NEXAFS) spectroscopy. Surface chemical properties of BARC films were derived from contact angle measurements of various liquids on these thin films. Preliminary results from these studies indicate that some BARC components may migrate to the BARC-resist interphase and act as dissolution inhibitors. Similarly, small molecule additives in the resist may migrate into the BARC layer, causing chemical modifications.

Keywords: BARC, resist, interphase, interfacial interactions, residual layer, NEXAFS, surface chemistry

1. INTRODUCTION

Bottom anti-reflective coatings (BARCs) are now used extensively in optical microlithography to improve process latitudes. By minimizing standing waves, thin film interference effects, and reflective notching from substrate reflections, BARCs provide better resolution and critical dimension (CD) control[1,2]. As the minimum feature size is shrinking to keep up with Moore's law, the exposure wavelength of microlithography tools continues to decrease from 248 nm to 193 nm. Subsequently, the exposure will be carried out at the vacuum UV (VUV) wavelength of 157 nm for sub-70 nm features. With decreasing exposure wavelength the optical interference effects due to substrate reflection become more severe as the reflectivity of the silicon (Si) substrate in general increases with decreasing wavelength. Hence, the importance of BARCs in integrated circuit (IC) manufacturing becomes more pronounced and valuable with decreasing feature size (wavelength).

Though BARCs play a major beneficial role in microlithography by minimizing or eliminating the optical interference effects, they are also source of unwanted problems by interacting or intermixing with the overlying resist layer. The chemically amplified photo-resists that are used in deep UV (DUV, i.e.; 248 and 193 nm exposure) lithography are prone to interfacial interactions, which lead to deviations in the resist profile such as footing, undercut, and pattern collapse[3-5]. It is desirable to obtain orthogonal and undistorted resist profiles after developing; as shown in Figure 1, deviations often

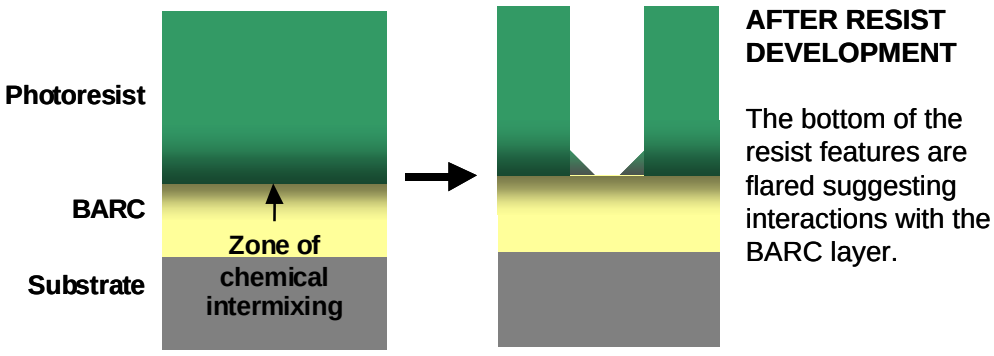

Figure 1. Interactions between polymer BARCs and chemically amplified photo-resists leads to a loss of resist feature size control and a reduction in resist feature quality.

result at the BARC-resist interface. The photo-acid generated upon exposure of the resist or small molecule additives present in the resist may diffuse into the underlying BARC layer during one of the thermal processing steps of the resist. Alternatively, small molecules such as acid catalyst, crosslinker, and other additives present in the organic BARC may migrate into the resist layer. Despite suppressing this diffusion and migration to a large extent by crosslinking the organic BARC, interactions between BARC and resist still occur. In addition to these chemical interactions, polymer chains in the resist may interdiffuse into the BARC layer leading to physical intermixing. It is essential to minimize the adverse interactions and make the BARC and resist materials more compatible, to obtain undistorted resist profiles.

This paper addresses these important and complex BARC-resist interfacial interactions. The main objectives of this study are to understand and characterize these interfacial interactions to provide guidance for the design and formulation of BARCs with minimal interactions so that BARC and resist may have mutual compatibility. To address these issues, the surface vs. bulk chemical properties of BARC and interlayer films were characterized using near edge x-ray absorption fine structure (NEXAFS) spectroscopy[6]. The change in surface chemistry of the BARCs was determined by measuring the contact angles of various liquids on BARC films. The thickness of interlayer, the residual layer over BARC after development of resist, was studied as a function of BARC cure temperature, crosslink density, and exposure dose. Dependence of resist profile on the thermal processing conditions of resist was studied by conducting a series of experiments with varying post application bake (PAB) temperatures and post exposure bake (PEB) temperatures. To observe the effect of BARC components on the interlayer thickness, a detailed study was carried out by spiking the resist formulation with different components of BARC and measuring the interlayer thickness after resist development.

2. EXPERIMENTAL

2.1 Materials

Two BARC formulations, BARC A and BARC B, were chosen for this study. 248 nm resists of each type, viz.; t-Boc (APEX-E Shipley), ESCAP (UV6 Shipley) and Acetal (SEPR503 Shin-Etsu), were studied. The crosslinkers were received from Cytec and used as received.

2.2 Near Edge X-ray Absorption Fine Structure (NEXAFS) spectroscopy

NEXAFS measurements were conducted at the U7A beamline of the National Synchrotron Light Source at Brookhaven National Laboratory. A monochromator with 600 line/mm grating, providing ≈ 0.15 eV resolution, was used for all the NEXAFS spectra. The monochromator energy scale was calibrated by the carbon *K*-edge π^* transition of graphite at 285.35 eV. All spectra were recorded at room temperature in the NIST – Dow material characterization chamber[6] at 10^{-6} Pa. The sample is exposed to polarized x-ray radiation from the synchrotron light source. The spectra are normalized to the incident beam intensity, I_0, by collecting the total electron yield intensity from a gold coated 90 % transmitting grid placed in the incoming X-ray beam path. The carbon fluorescence yield was measured with a differentially pumped

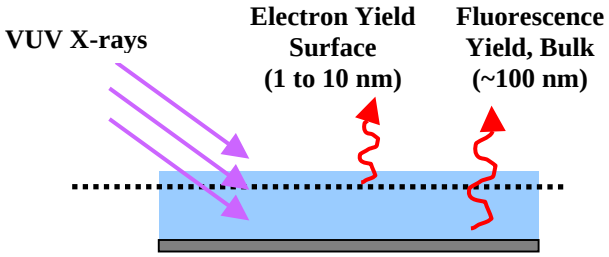

Figure 2. NEXAFS Schematic. VUV X-rays are preferentially absorbed by the sample when the incident radiation is at the appropriate energy to excite a core shell electron to an unoccupied molecular orbital, causing the emission of Auger electrons from up to 10 nm into the film (surface) and photons from up to 100 nm into the film (bulk).

UHV compatible proportional counter filled with 2.67 x 10^4 Pa of P-90 (90 % methane, 10 % argon) in an energy dispersive mode to reduce background fluorescence from other elements. Surface sensitive partial electron yield measurements are made (probe depth of approximately 1 nm to 6 nm) by applying a negative bias on the entrance grid of the channeltron electron detector. For the carbon K-edge spectra (260 to 330) eV, the electron yield detector was set with negative bias of 50 V, 100 V, 150 V, 200 V, and 250 V for surface depth profiling, described below. The spectra were collected with the incident beam at the magic angle (54.7^o) relative to the sample in order to remove any polarization dependence. For the NEXAFS spectra in this paper the experimental standard uncertainty in the peak position is similar to the grating resolution of ± 0.15 eV. The relative uncertainty in the NEXAFS intensity is less than ± 5% and was determined by multiple scans on a sample.

A schematic of the NEXAFS experiment is shown in Figure 2. VUV X-rays are preferentially absorbed by the sample when the incident radiation is at the appropriate energy to allow the excitation of a core shell electron to an unoccupied molecular orbital. Due to the well-defined energy gap associated with a core shell to unoccupied orbital transition, NEXAFS is sensitive to the bonding characteristics of the atom giving a discrete peak for each chemical bonding environment. During electronic relaxation Auger electrons and characteristic fluorescence photons are emitted from the irradiated sample. The electronic relaxation processes may release more than one electron. The electrons emitted deep within the film cannot escape; only the electrons emitted near the top (1 nm to 6 nm) of the film surface have enough energy to escape the surface potential. The photons have a longer escape depth of ≈100 nm within the bulk of the sample. The electron yield detector has a grid where a negative voltage bias can be applied. The electrons that escape the surface of the film, but are emitted from furthest within the film are low in energy due to inelastic interactions with other atoms. These low energy electrons do not have enough kinetic energy to pass the negative detector bias and are not detected. If the negative detector bias is gradually increased, progressively higher energy electrons are detected, and the effective electron yield sampling depth gets closer to the film surface. In this way, depth profiling is accomplished by varying the voltage bias across the detector grid. NEXAFS measurements were conducted on the BARC films, deprotected polymer on BARC, and BARC + residual layer as a function of the electron yield detector bias. For the residual layer studies, the soluble resist portion of the film was removed (developed) after PEB by immersion in aqueous base developer.

2.3 Contact Angle Measurements

The contact angle data for the two BARC coatings was studied with four liquids, each with different acid and base components to the surface tension. The BARC films were cured at different temperatures ranging from (150 to 250) ^{o}C. The contact angle measurements are static contact angles. A drop of the fluid was placed on the BARC surface from a pipette and the contact angle immediately measured. The contact angles reported are an average from measurements on both sides of at least 9 different droplets. The relative uncertainty in the contact angle measurements is ± 2.5 degrees and is dominated by the uncertainty of determining the tangent line to the droplet near the substrate. The standard deviation from the 9 measurements was usually ≈ 1 degree.

2.4 Ethyl Lactate (EL) Stripping Test

A wafer was spin coated with BARC and baked at 205 °C for 60 s and the thickness of the BARC layer was measured using a single wavelength ellipsometer. The wafer was placed on the spinner and EL was puddled on the wafer for 10 s and spun at 3000 rpm for 20 s. The thickness was measured again and any decrease in thickness was considered to be

due to the stripping of BARC layer. No loss of thickness indicates the robustness of the BARC film and completion of the crosslinking reaction.

2.5 Interlayer Thickness Measurements:
A Si wafer was spin coated with BARC and baked at 205 °C for 60 s and the thickness of the BARC layer was measured using a single wavelength (632.8 Å) J. A. Woollam ellipsometer. Photoresist was spin coated over the BARC layer and subsequent processing steps of PAB, exposure, PEB, and developing were carried out according to the standard procedure for the given resist. The thickness was measured again using the ellipsometer. The difference (final – initial) was taken as the thickness of interlayer.

2.6 Lithography and Imaging:
Resist was spin coated on a BARC-coated silicon wafer and softbaked (PAB) at the required temperature. Exposures were carried out using a 248 nm Microscan 3 (SVGL-ASML) scanner with numerical aperture (NA) of 0.6 and coherence (σ) of 0.65. The PEB temperature and time were varied to observe its effect on resist profile. The exposed resist was developed in a PD523AD developer for 60 s. Imaging was done at Brewer Science with a Leo (Model 1560) scanning electron microscope (SEM). The cross-sectional imaging was carried out with a tilt angle of 75°.

3. RESULTS AND DISCUSSION

3.1 Surface versus bulk chemistry of BARC materials as a function of cure temperature.
Acids generated during UV exposure catalyze the deprotection reaction responsible for the solubility switch for positive-tone chemically amplified resists. Since the deprotection reaction is sensitive to acid concentration, surface interactions between the BARC and photo-generated acid are a potential cause of the footing/undercut phenomena. For example, basic functional groups on the BARC surface could slow the deprotection reaction by neutralizing acid in the BARC-resist interfacial region, leading to footing. Conversely, acidic groups on the BARC surface can potentially promote the deprotection reaction, causing undercut. The BARCs considered here are cross-linked polymer networks. The BARC surface chemistry is expected to be dependent on the curing conditions; small molecule and short chain segregation to the BARC surface can potentially cause changes in the surface chemistry, controlled by a competition between surface segregation and the curing reaction, which will slow the segregation process. One observation is that the severity of the footing/undercut deviations is dependent on the curing temperature. NEXAFS and contact angle measurements were used to probe for changes in BARC surface chemistry as a function of cure temperature, with the hypothesis that surface chemical differences are potential factors that induce deviations in the pattern profile. In addition, if surface segregation is a significant factor, chemical differences in the surface depth profile should be observable using the NEXAFS surface depth profiling technique described above.

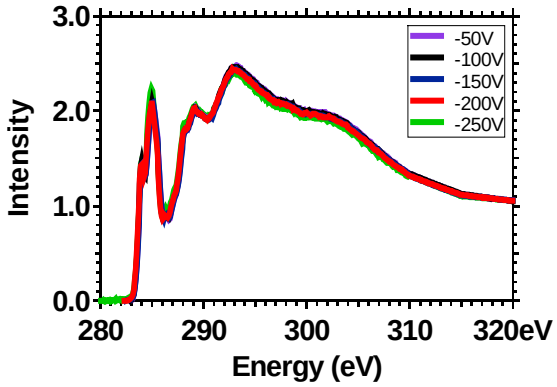

Figure 3. NEXAFS Carbon *K* Edge Electron Yield (Surface) Spectra of BARC A, Surface Depth Profiles, T_{Cure} 205 ºC

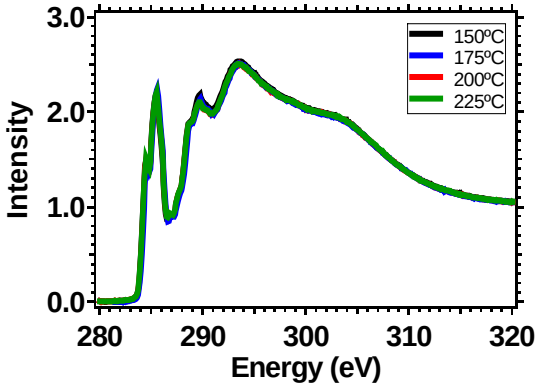

Figure 4. NEXAFS Carbon *K* Edge Electron Yield (Surface) Spectra of BARC A, Variable T_{Cure}, -150 V Detector Bias

NEXAFS is a very sensitive technique that can provide accurate information about the chemical environment of individual atoms in a film. The NEXAFS carbon *K*-edge electron yield spectra of the surface of BARC A cured at 205-°C at different bias voltages, both pre- and post-edge jump normalized, are shown in Figure 3. Post-edge normalization eliminates the spectral dependence on total carbon content, therefore, changes in the NEXAFS spectra are indicative of changes in the chemical functionality. In the figure, the spectrum at -250 V corresponds to the top surface of the BARC. The chemical composition of the surface does not change from 1 nm to 6 nm. Figure 4 shows the carbon *K*-edge electron yield spectra for BARC A under the different cure conditions. All of the spectra overlap indicating no changes in the surface chemical functionality with cure temperature. The edge jump intensities for the BARC at different cure temperatures were also the same, within experimental error, indicating no changes in the relative amounts of carbon in the surface sampling volume. Since the footing/undercut problem is *dependent* on the BARC cure temperature, and the surface chemistry was *independent* of BARC cure temperature, this suggests that acid/base neutralization reactions from the BARC surface are not a significant factor for footing or undercut with these BARC-resist systems. The data in Figure 5 shows that the contact angles do not change with the BARC cure temperature. Also the contact angles are the same for both BARC A and BARC B in each of the fluids.

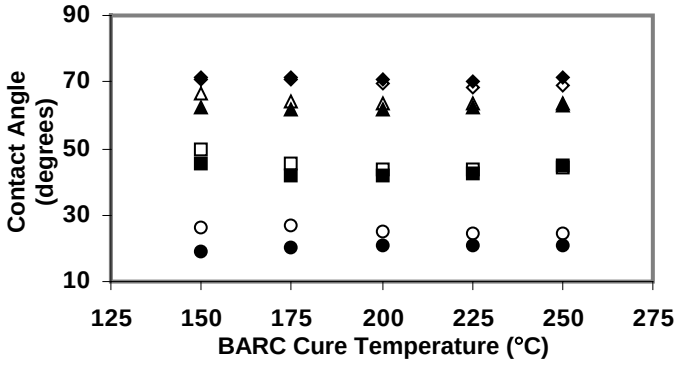

Figure 5. Fluid Contact Angles of Various Liquids Measured on BARC Surfaces, Variable Cure Temperature, closed symbols correspond to BARC A, open to BARC B; ● diiodomethane, ■ ethylene glycol, ▲ glycerol, ♦ water.

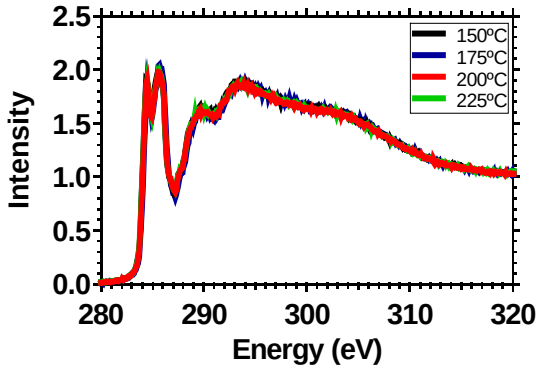

Figure 6. NEXAFS Carbon *K* Edge Fluorescence Yield (Bulk) Spectra of BARC A, Variable T_{cure}

Since the contact angle data can be related to the acid and base components of the BARC surface tension, Figure 5 further suggests that the acidity/bacisity of the BARC surface is not critical for footing or undercut. In addition, the fluorescence yield NEXAFS spectra shown in Figure 6 demonstrate that there are no changes in the bulk of the BARC film with cure temperature. The NEXAFS and contact angle data show no BARC surface chemistry dependence on cure temperature, leading to consideration of other potential causes of the footing/undercut problems. The dependence of the footing/undercut phenomena on BARC cure temperature is possibly caused by interdiffusion between BARC and resist components. For example, the photo-acid generator may diffuse into the BARC coating. The acid catalyst used to promote BARC curing or unreacted BARC components can diffuse into the resist and cause contamination.

As inter-layer (IL) (the residual resist layer over BARC after developing, also called residual layer) thickness is considered to be an indicator of BARC-resist interactions, IL thickness was studied as a function of cure temperature. IL thickness of all three resists, APEX-E, UV6 and SEPR503 over BARC A and BARC B were measured. The cure temperature was varied from 145 °C to 225 °C and the values of IL thickness are listed in Table I. As can be seen from the table, the thickness is *independent* of cure temperature for both BARCs. This lack of IL dependence on cure temperature in this study may be due to the fact that the crosslinking reaction might have been completed even at the low temperature of 145 °C.

Table I. IL thickness of BARCs with different cure temperatures (error ± 1 nm)

Temperature	APEX-E		UV6		SEPR 503	
	BARC A	BARC B	BARC A	BARC B	BARC A	BARC B
145 °C	2.1 nm	2.6 nm	2.2 nm	3.1 nm	2.4 nm	3.2 nm
165 °C	2.3 nm	1.8 nm	2.2 nm	2.3 nm	2.1 nm	2.4 nm
185 °C	2.1 nm	2.1 nm	2.2 nm	2.2 nm	2.3 nm	2.1 nm
205 °C	2.3 nm	2.1 nm	2.3 nm	2.0 nm	2.6 nm	2.0 nm
225 °C	1.9 nm	4.1 nm	2.7 nm	1.8 nm	2.2 nm	2.0 nm

3.2 Dependence of the thickness and composition of the residual layer on BARC components.
BARC components (catalyst or cross-linker) are added to the resist or are present in excess in the BARC to see if they affect resist performance. If a significant residual layer exists after exposure and bake, then transport of that component from the BARC to the resist can contribute to footing. If no residual layer is present after only PAB, then catalyst transport can contribute to undercut. The chemical composition of residual layers are analyzed with NEXAFS; the spectra provides information about whether the resist is deprotected or not (dissolution inhibition or inhibited deprotection) or if any BARC components have segregated from the BARC into the resist layer. Figure 7 shows a schematic of the typical configuration and preparation of a residual layer sample.

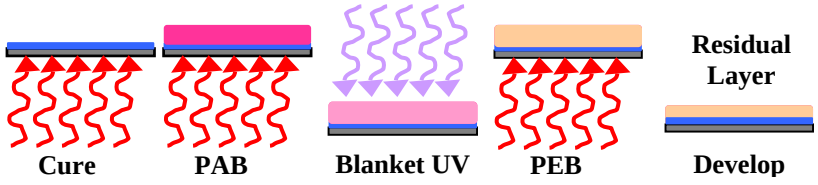

Figure 7. Residual layer experiments sample preparation. Experiments are designed to investigate the effect of BARC components on resist performance as a function of standard processing steps.

It was hypothesized that the BARC-resist interactions may arise from the reactions induced by small molecules that diffused from BARC to resist layer. To test this hypothesis, individual components of BARC, such as acid catalysts and crosslinkers, were added to a resist formulation APEX-E and their effect on IL thickness was examined. Table II shows the interlayer thickness of APEX-E resist over BARC A in two different processing conditions. In one case a post apply bake (PAB) at 90 °C was carried out and followed by developing the resist with usual TMAH developer. In the other case, the processing conditions include PAB, exposure, post exposure bake (PEB) and developing. With the addition of mass fraction 0.05 % of catalyst1 and PAB at 90 °C the resist was completely developed without any exposure. This clearly indicates that the resist was deprotected during the PAB at 90 °C. The interlayer thickness did not change very much when the process of exposure and PEB were added. In the case of another catalyst, catalyst2, the deprotection of the resist polymer was not complete during the heating alone. Since catalyst2 is a thermal acid generator it would not have produced sufficient acid at 90 °C to effect adequate deprotection. When mass fraction 0.65 % of crosslinker1 was added to the resist formulation and PAB at 90 °C was carried out, there was no change in the resist thickness after developing. However, after exposure, PEB, and developing, the resist remained without any dissolution. This inhibition of dissolution can be ascribed to the neutralization of the photo-acid generated on exposure by crosslinker1, which is basic in character due to the presence of three *tertiary*-amino groups in the molecule. When the resist formulation was spiked with mass fraction 0.37 % crosslinker2 the resist thickness remained the same after PAB and developing. But, the residual resist thickness of ≈300 Å was measured after exposure, PEB and developing. Crosslinker2, being less basic than crosslinker1, was unable to neutralize the large quantity of photo-generated acid and hence the interlayer was thinner. Addition of other additives like catalyst3 and catalyst4 (both weak acid catalysts) and FSO-100 (surfactant) did not have any significant observable effect on the interlayer thickness.

Table II. IL Thickness with APEX-E Resist Spiked with Components of BARC (error ± 1 nm)

Resist processing Conditions			
Post Apply Bake	No	90 ºC/60s	90 ºC/60s
Exposure dose	No	No	30 mJ/cm^2
Post Exposure Bake	No	No	90 ºC/90s
Over BARC A	in nm	in nm	in nm
APEX-E + 0.05% Catalyst1	540	1.7	2.6
APEX-E + 0.05% Catalyst2	710	585	2.4
APEX-E + 0.65%Crosslinker1	956	896	917
APEX-E + 0.37% Crosslinker2	890	890	29.5
APEX-E + 0.14% Catalyst3	910	910	2.2
APEX-E + 0.14% Catalyst4	940	885	2.3
APEX-E + 0.1% FSO-100	900	939	2.6

As a control, the series of experiments was repeated with poly(hydroxystyrene) (PHS) (a model resist polymer) instead of APEX-E resist formulation. The results are summarized in Table III. Addition of catalyst1, crosslinker1 or crosslinker2 alone did not influence any effect on the IL thickness under both processing conditions. However, with the combination of catalyst1 and crosslinker1 or catalyst1 and crosslinker2 the residual thickness was large. In the presence of acid catalyst, crosslinker1 and crosslinker2 must have undergone crosslinking reaction with PHS.

The results reveal very interesting insights into the BARC-resist interactions. As indicated by the spiking experiment with catalyst1, if any acid migrated to the resist layer from BARC it could deprotect the polymer during PAB even in the unexposed area and thus leading to undercut of the resist profile. Similarly, the lack of dissolution in the presence of

Table III. IL Thickness with PHS Spiked with Components of BARC (error ± 1 nm)

"Resist" processing Conditions			
Post Apply Bake	No	130 ºC/60s	130 ºC/60s
Exposure dose	No	No	30 mJ/cm^2
Post Exposure Bake	No	No	130 ºC/90s
Over BARC A	in nm	in nm	in nm
PHS	1.0	1.2	1.9
PHS + 0.05% Catalyst1	1.0	2.3	2.7
PHS + 0.65%Crosslinker1	1.1	1.9	1.7
PHS + 0.37% Crosslinker2	0.7	1.4	1.5
PHS + 0.025% Catalyst1+0.33% Crosslinker1	0.7	27.5	364
PHS + 0.025% Catalyst1+0.33% Crosslinker2	0.5	147	157

Figure 8. Chemical structures of model basic compounds

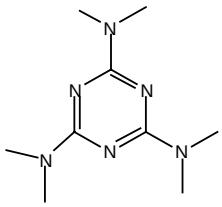

2,4,6-Tris(dimethylamino)-1,3,5-triazine

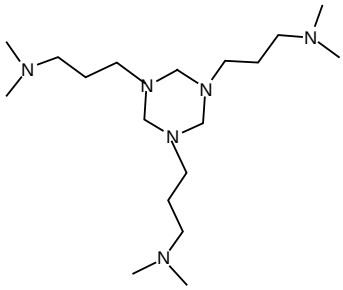

1,3,5-Tris[3-(dimethylamino)propyl] hexahydro-1,3,5-triazine

basic crosslinker1 shows that strong basic components like crosslinker1 can neutralize the photo-acid generated during irradiation and lead to footing problem. The control experiments with PHS clearly showed that acid neutralization and not the crosslinking reaction induced by basic component causes the lack of dissolution of the resist during developing.

To confirm the conclusion that the lack of dissolution of resist in the presence of crosslinker1 is due to the neutralization of the photo-acid by the basic crosslinker1, the spiking experiments were carried out with two model basic compounds that are structurally similar to crosslinker1. The chemical structures of the model compounds, 2,4,6-Tris(dimethylamino)-1,3,5-triazine and 1,3,5-Tris[3-(dimethylamino)propyl]hexahydro-1,3,5-triazine, are shown in Figure 8. These compounds have cyclic structure similar to crosslinker1 and each possesses three tertiary amino groups. Just like with crosslinker1, these model basic additive compounds induce lack of dissolution of the resist after exposure and development. The values of IL thickness of APEX-E resist spiked with model basic compounds over BARC A are collected in Table IV. This result unequivocally shows the neutralization of the photo-acid is the reason for lack of dissolution of the resist.

Table IV. IL Thickness with APEX-E Resist Spiked with Model Additives over BARC A (error ± 1 nm)

Resist processing Pre-bake Exposure dose Post Exposure bake	 90ºC/60sec No No	 90ºC/60sec 30mJ No	 90ºC/60sec 30mJ 90ºC/90sec
1,3,5-Tris[3-(dimethylamino) propyl]hexahydro-1,3,5-triazine	1320 nm	1380 nm	1242 nm
2,4,6-Tris(dimethylamino)-1,3,5-triazine	774 nm	876.2 nm	856.1 nm

Additional investigation of the effect of spiking BARC with excess BARC components (catalyst and crosslinker) was performed using NEXAFS to compare the surface of typical formulation BARC and resulting residual layer with spiked BARC and resulting residual layer. As shown in Figures 9 and 10, NEXAFS carbon *K*-edge electron yield spectra taken at –250 V bias for the residual layer of regular formulation BARC A and BARC A formulated with excess crosslinker, the residual layer (center spectrum) is a combination of peaks from both developed resist and BARC A, indicating that BARC components migrate to the surface of the residual layer where, as mentioned above, it is possible that the crosslinker interacts with the resist and acts as a dissolution inhibitor. In Figure 10, the residual layer has a distinct peak at ≈289 eV, corresponding to excess crosslinker on the residual layer surface.

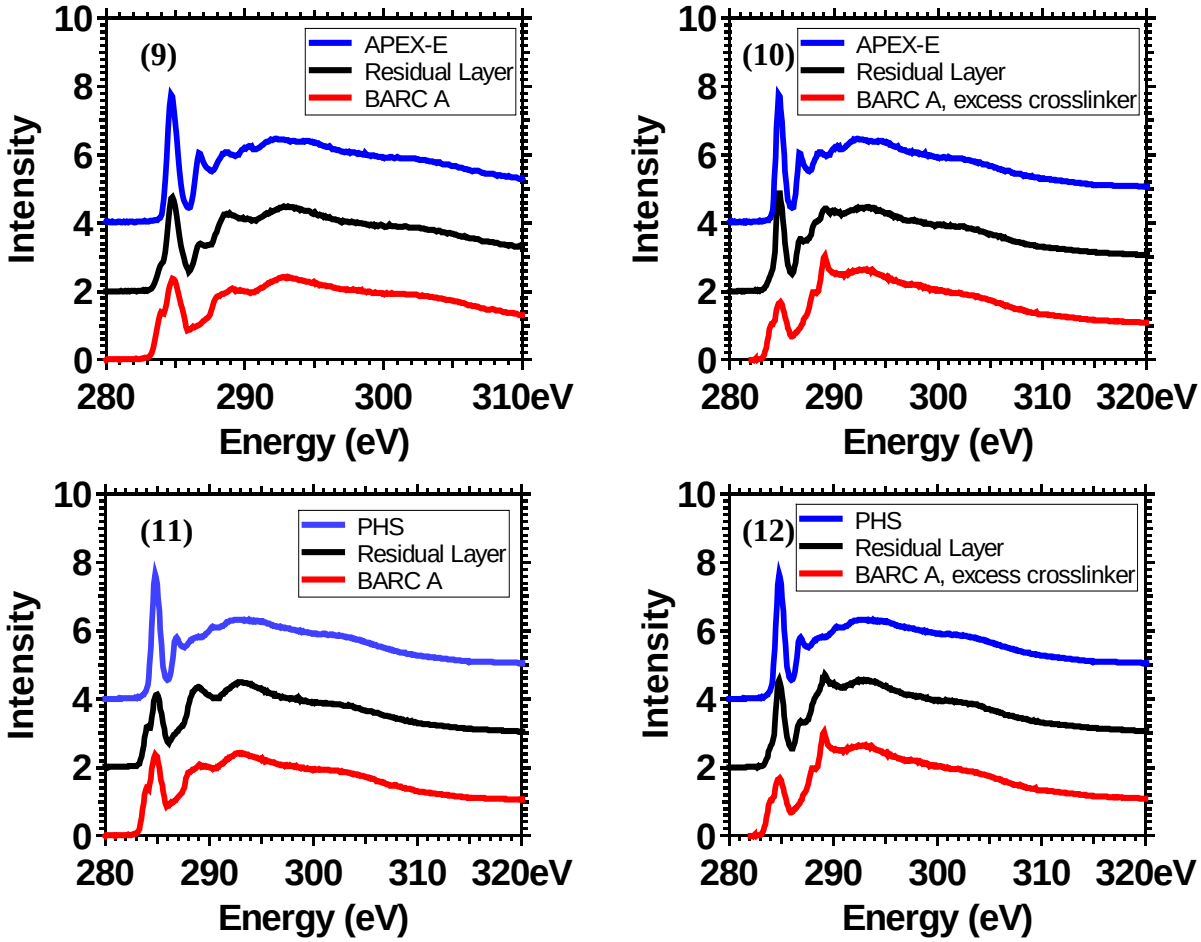

Figures 9-12. NEXAFS Carbon *K* Edge Electron Yield (Surface) Spectra. (9) Residual layer of APEX-E on BARC A; (10) Residual layer of APEX-E on BARC A with excess crosslinker; (11) Residual layer of PHS on BARC A; (12) Residual layer of PHS on BARC A with excess crosslinker

Similar results are shown in Figures 11 and 12, indicating that dissolution inhibition by the crosslinker has led to residual layer formation. These spectra are of PHS over BARC A. PHS, being completely deprotected, should develop completely regardless of treatment and presence of acid catalyst. However, we again see that the residual layer spectra are a combination of both resist and BARC A, especially for the case shown in Figure 12, having excess crosslinker.

3.3 Dependence of residual layer thickness on crosslink density, bake temperature, and exposure dose.

A study to observe the effect of crosslink density on the IL thickness was carried out by varying the polymer/crosslinker mass ratio in both BARCs. For instance, the polymer/crosslinker2 ratio in BARC A formulation was changed from a high crosslinker loading of (1/1) to very low (20/1). In the BARC B formulation, the polymer/crosslinker1 ratio was varied from high (1/1) to low (10/1). For all the formulations the baking temperature was kept at 205 °C with a baking time of 60 s. The values of IL thickness for modified formulations with APEX-E resist are collected in Table V. As Table V shows the IL thickness is insensitive to the crosslink density in the modified BARC A formulations except in the case of very low crosslinker2 concentration. With the 20/1 ratio of polymer/crosslinker2 the BARC coating was stripped during developing of resist. This stripping of layer can be ascribed to insufficient crosslinking due to very low crosslinking concentration in the formulation. The EL stripping test also confirmed the insufficient crosslinking in that formulation. In the case of modified BARC B formulations, the crosslink density did not have any effect on IL thickness.

Table V. IL thickness of BARCs with different crosslink density with APEX-E (error ± 1 nm)

Polymer/ Crosslinker2	BARC A, nm	Polymer/ Crosslinker1	BARC B, nm
1.0/1.0	3.1	1.0/1.0	1.8
5.3/1.0	2.2	2.8/1.0	1.6
7.3/1.0	23	3.8/1.0	2.6
9.3/1.0	1.9	4.8/1.0	1.7
20/1.0	-22.3	10/1.0	2.0

Even with the (10/1) ratio of polymer/crosslinker1 the coating did not show any stripping. As crosslinker1 has more crosslink sites and is a more efficient crosslinker, even this low concentration of crosslinker1 is enough to effect complete curing and thus robust film. As with APEX-E, other two resists UV6 and SEP503 produced similar results of lack of dependence of IL thickness on crosslink density. Variation of bake temperature with these modified formulations also did not indicate any dependence on crosslink density.

Another study to find the effect of exposure dose on IL thickness was carried out by changing the dose from 30 mJ/cm^2 to 500 mJ/cm^2. The dependence on dose for APEX-E is shown Figure 13. As the figure shows, the exposure dose did not have much effect on IL thickness up to 150 mJ/cm^2. At doses above this value the IL thickness increases with dose, particularly at 500 mJ/cm2 the thickness is doubled.

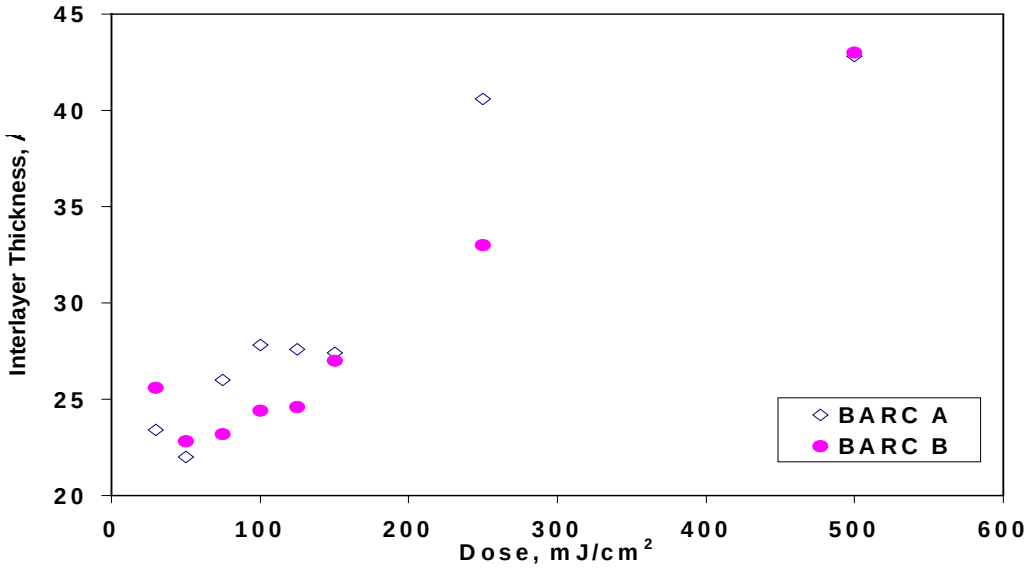

Figure 13. Dependence of IL thickness on exposure dose for APEX-E resist, error ± 1nm).

In general, there is no appreciable dependence of IL thickness on either bake temperature or crosslink density or exposure dose up to 150 mJ/cm^2. This lack of dependence on key parameters is surprising. Since the bake temperature is expected to influence the curing reaction and thus the extent of crosslinking IL thickness vastly different from the normal value is expected for coatings baked at low temperature. One reason for this lack of dependence is that the low bake temperature of 145 °C is high enough to effect full curing. Hence, a future study will be conducted with bake temperatures below 145 °C. Similarly, with crosslinker1 the polymer/crosslinker1 ratio should be increased above

(10/1) to observe the effect of crosslink density on IL thickness. Another unexpected result is that for both BARC A and BARC B the thickness of IL is not very different even though they show different resist profile behavior. Since the PEB temperature as well as the PEB time have profound effect on the resist profile a systematic study of the influence of PEB time and temperature on litho profile was carried out. The PEB temperature and time were varied in a large range and the SEM images were compared. As far as the resist profiles are concerned, the expected trend was observed. With lower PEB temperature and time than the required values, the profile was underdeveloped since the deprotection reaction would be incomplete. With valued higher than the prescribed values the resist profiles were thinner than the mask size as the deprotection reaction would have spread to unexposed areas. However, one unusual effect was observed while analyzing the SEM images. As shown in Figure 14, for UV6 resist over BARC B at a PEB temperature of 110 °C with short PEB times the adhesion of the BARC layer to the Si substrate and of resist to the BARC layer appears to be very weak. The layers seem to be delaminated and with increasing PEB time the adhesion seems to improve and layers are more homogeneous. This warped layer structure was observed for other PEB temperatures also. This shows that the interactions between BARC layer and resist layer continue to occur during the thermal processing steps of the resist.

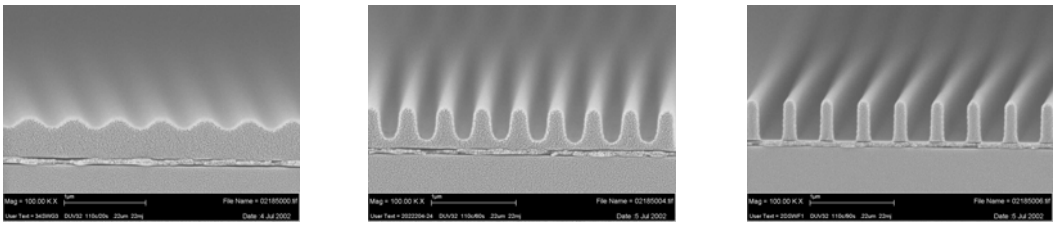

PEB 110 °C/20 s PEB 110 °C/60 s PEB 110 °C/90 s

Figure 14. SEM images of UV6 resist over BARC B profile at different PEB times at 110 °C

4. CONCLUSIONS

The interlayer thickness was studied as a function of BARC cure temperature, crosslink density, exposure dose, and resist bake temperature. Dependence of IL thickness on these factors is minimal. Hence, IL thickness may not be the true indicator of the BARC-resist interfacial interactions. Spiking experiments clearly showed that if any basic component migrated from BARC to resist it could neutralize the photo-acid or inhibit dissolution and lead to footing in the resist profile. Similarly, if any acid species diffuses to resist it can deprotect the resist polymer in unexposed region and thus leading to undercut of resist profile. NEXAFS spectral data indicate that catalyst2, the acid catalyst in BARC A, can migrate to the top surface of the IL.

ACKNOWLEDGMENTS

The authors thank the Missile Defense Agency (MDA) for the financial support through Phase II program Contract #DASG60-1-C0047, and wish to acknowledge Mr. Michael Rich of Brewer Science and SEMATECH for the lithography work. ELJ acknowledges support by NRC-NIST postdoctoral fellowship.

REFERENCES

1. J. E. Lamb III, *Semiconductor Fabtech*, **2**, 223-227,1995.
2. J. Sturtevant, B. Roman, *Microlithography World*, 13-21, Autumn 1995.
3. H. Yoshino, T. Itani, S. Hashimoto, M. Yamana, T. Yashii, H. Tanabe, *Proc. SPIE*, **3333**, 655-665, 1998.
4. H. B. Cao, P. F. Nealey, W-D. Domke, *J. Vac. Sci. Technol. B*, **18**, 3303-3307, 2000.
5. J. Simons, D. Golfarb, M. Angelopoulos, S. Messick, W. Moreau, C. Robinson, J. De Pablo, P. Nealey, *Proc. SPIE*, **4345**, 19-29, 2001.
6. J. L. Lenhart, R. L. Jones, E. K. Lin, C. L. Soles, W-L. Wu, D. L. Goldfarb, M. Angelopoulos, , *J. Vac. Sci. Technol. B*, **20**, 2920-2926, 2002.